Modeling the large-scale geometry of human coronary arteries

Mark A. Changizi and Christopher Cherniak

Abstract: Two principles suffice to model the large-scale geometry of normal human coronary arterial networks. The first principle states that artery diameters are set to minimize the power required to distribute blood through the network. The second principle states that arterial tree geometries are set to globally minimize the lumen volume. Given only the coordinates of an arterial tree's source and "leaves", the model predicts the nature of the network connecting the source to the leaves. Measurements were made of the actual geometries of arterial trees from postmortem healthy human coronary arteriograms. The tree geometries predicted by the model look qualitatively similar to the actual tree geometries and have volumes that are within a few percent of those of the actual tree geometries. Human coronary arteries are therefore within a few percent of perfect global volume optimality. A possible mechanism for this near-perfect global volume optimality is suggested. Also, the model performs best under the assumption that the flow is not entirely steady and laminar.

Key words: arteries, optimization, volume, power, geometry.

Résumé : On peut modéliser la géométrie d'un réseau d'artères coronaires humaines normales en faisant appel à deux principes. Le premier veut que les diamètres artériels soient tels qu'ils minimisent le travail nécessaire pour distribuer le sang à travers le réseau. Le second veut que la géométrie de l'arbre artériel soit telle qu'elle minimise globalement le volume de la lumière. S'appuyant uniquement sur les coordonnées de source et de terminaisons d'un arbre, le modèle peut alors prédire le réseau. Les géométries réelles d'arbres artériels sains, obtenus par coronarographie post-mortem chez des humains, ont été mesurées. Les géométries prédites par le modèle sont qualitativement similaires aux géométries réelles et ont des volumes correspondant à un pourcentage près à ceux des géométries réelles. Ainsi, les artères coronaires humaines ont une optimalité de volume global presque parfaite. On suggère un mécanisme possible pour cette optimalité presque parfaite. Le modèle est meilleur sous l'hypothèse que l'écoulement n'est pas entièrement stationnaire et laminaire.

Mots clés : artères, optimisation, volume, travail, géométrie.

[Traduit par la Rédaction]

Introduction

Optimality principles have often been applied to the diameters and branching angles of arterial junctions at least since the work of Murray (1926*a*,*b*), the prediction being that the observed diameters or branching angles are such that they optimize some magnitude. The large-scale geometry of arterial networks has been little studied in the light of these optimality principles, with the exception of Kamiya and Togawa (1972) who found the locally optimal tree for one mesenteric tree in a dog and Schreiner and Buxbaum (1993) and Schreiner et al. (1994, 1996) who built model vascular trees by iteratively adding locally optimal 'Y' junctions. The research presented here is the first to employ algorithms capable of predicting the arterial tree given only the coordinates of the source and leaf segments. We were able to show the extent to which global optimality principles concerning pumping power, drag force, volume, and surface area predict the actual geometry of multiple-leaf arterial tree networks. (The large-scale geometry of dendrites and axons has been studied using these optimality principles by Cherniak et al. 1999.)

The remainder of this introduction is divided into two sections. The first covers Murray's Law and variants, derived via a principle of power optimization, which lead to equations of the form $d_0^p = d_1^p + d_2^p$, where d_0 is the parent's, or trunk's diameter, and d_1 and d_2 are its childrens' diameters. We argue that values of p ought be considered within the range [2,3]. Equations of this form will be used in order to assign diameters to trees so that their pumping power cost, drag force cost, volume cost, or surface area cost may be calculated. These latter four principles are introduced in the second section of the introduction and were used in order to determine arterial tree geometries which were compared with actual arterial geometries. For example, we compared global volume-optimal tree geometries to actual tree geometries and observed close quantitative and qualitative agreement.

Received November 8, 1999. Published on the NRC Research Press web site on July 14, 2000.

M.A. Changizi.[1] Department of Computer Science, National University of Ireland, Cork, Ireland.

C. Cherniak. Committee on the History and Philosophy of Science, Department of Philosophy, University of Maryland, College Park, MD 20742, U.S.A.

[1]Author for correspondence at the Department of Neurobiology, Duke University Medical Center, Box 3209, Durham, NC 27710, U.S.A. (e-mail: changizi@cs.ucc.ie).

Principle of minimum pumping power and diameter determination

Under the assumption that blood flow obeys Poiseuille's Law, Murray (1926*a*) derived that for arterial networks minimizing pumping power, the volumetric flow rate in an arterial segment is proportional to the cube of the diameter: this is called Murray's Law. [Hess (1917) was apparently the first to derive this result.] Let the depth of a branch segment in an arterial tree be the number of branch junctions away from the single source segment. Since the flow through a fluid network must be conserved, the sum of the flow in all arterial segments at the same depth must be the same across depths, e.g., the flow through the superior mesenteric artery equals the flow through all its grandchildren segments. By Murray's Law this is to say that Σd^3, where the summation is over all cubed diameters of segments at a given depth in the network, is constant across all depths. A corollary of this is that the diameter of a single parent segment is related to those of its children by $d_0^3 = \Sigma d_i^3$, where d_0 is the diameter of the parent segment (or trunk) and each d_i is a child segment diameter. If one knows the diameters of each leaf segment of a tree, this last version of Murray's Law is a powerful tool in that it allows one to obtain the optimal diameters for every non-leaf segment. [LaBarbera (1990) proposed a local shear stress-dependent mechanism for explaining how arterial networks conform, to the extent that they do, to Murray's Law.] More generally, we presume that diameters are set so as to minimize the required pumping power and that the resulting parent to child diameter relationship is given by the general formula $d_0^p = \Sigma d_i^p$ for some $p \in [2,3]$ (see Discussion). We are supposing that p may possibly be any value in this range since the complete arterial network may be subject to a mixed story; i.e., some subnetworks may be partially steady, partially laminar, or both. Note that this d^p rule, for any p, is just as strong a tool as Murray's Law for obtaining non-leaf branch segment diameters given the leaf diameters.

Roy and Woldenberg (1982) defended a d^p rule as well, summarily reporting that exponent values best fitting the actual diameter data tend to be highly variable. However, they allowed the exponent to range more widely than did we, and specifically to range below 2. Our background assumptions leading us to confine the exponent to [2,3] are therefore stronger than Roy and Woldenbergs', but seem justified for the following reasons: *i*) theoretically, as noted in Woldenberg and Horsfield (1983), when $p < 2$ the cross-sectional area of the parent is less than the sum of that of the children the volumetric flow rate accordingly increases, contradicting the eventual tendency for the flow rate to decrease in lower depths; and *ii*) empirically, other than in Woldenberg and Horsfield (1983) where more than half of 199 human pulmonary artery junctions in the diameter range 0.7–16.8 mm have a best-fit exponent < 2 for the actual diameters, other research confirms best-fit exponents nearer to 3, and certainly tending above 2 (see Discussion). On this latter note, Woldenberg and Horsfield in the same article report that 125 of the 199 junctions optimize surface area better than volume (and better than the other cost measures discussed below). This is predominantly a consequence of the unusually large proportion of best-fit exponent values below 2, because for these exponent values only the surface area optimization model predicts branch angles at all close to the observed angles (Woldenberg and Horsfield 1983), which tend to be in the range from 60° to 80° (see below).

The large-scale structure of an arterial network is that of a tree, and our goal was to model arterial trees. The trees we studied did not include all actual arterial depths below the source; rather, the trees were just subtrees of the full arterial network, and the leaves did not need to be at the same depth. For example, from among a depth–3 binary tree (i.e., with 8 leaves), we might consider the subtree consisting of the source, its two children, and the two grandchildren from just one child. Also, we studied only planar trees as global optimization of three-dimensional trees is not well understood. A full geometrical characterization of a tree, or tree geometry, specifies (*i*) the coordinates of the source and each leaf; (*ii*) the coordinates of each branch junction between source and leaves; and (*iii*) the connectivity relation over the set of the source, leaves and branch junctions (this specifies the tree's topology). In modeling a particular actual tree, the actual source and leaf coordinates are measured and assumed fixed, so that any predicted tree must also connect the fixed source to the fixed leaves. Predicted trees need satisfy no other geometrical constraint; they may make their branchings anywhere in the plane. Our task was thus reduced to determining (*ii*) and (*iii*) so as to closely approximate the actual tree. See Fig. 1A for terminology related to trees.

It was necessary that candidate tree geometries acquire diameters for their segments so that we could ultimately compute the tree geometry with the minimum, say, volume. In assigning diameter values to segments in candidate trees of non-actual topologies, there was a difficulty: the segments of trees of different topologies could not be put into any natural one-to-one correspondence. Consider Fig. 2. Suppose that (A) represents the actual geometry of the measured tree, and that the tree shown in (B) is another candidate tree, but of a different topology. In order to compare the costs of the two trees, each segment in each tree must be assigned a diameter. The leaf diameters in (B) can be set to whatever they are in (A), but what should the diameters of c and d be? c and d do not correspond to a and b. For this reason, it is not well-defined to set the diameters of segments in a candidate tree to the diameters of corresponding segments in the actual tree. A natural way of handling this dilemma is to presume that for any candidate tree geometry, whether it be that of the actual geometry or that of some predicted tree, the diameters are set according to the d^p rule for some $p \in [2,3]$; i.e., they are assumed to be power optimizing (see earlier discussion). The leaf diameters of any candidate tree connecting source to leaves are presumed to be that of the actual tree, and the non-leaf segment diameters (including the source segment diameter) are obtained by the d^p rule. (See Materials and methods for how the leaf diameters of the actual tree are determined.)

Principles of minimum volume and surface area and tree geometry determination

There are a class of optimality principles that predict, respectively, that the tree geometry is such that it minimizes the power (P) required to pump blood through the junction (Murray 1926*a*), the total drag force (D) along the endothelium (Zamir 1976*b*), the total lumen volume (V), and surface

Fig 1. Terminology concerning branching networks. A) This schematic diagram depicts the measured portion of an arterial tree. In addition to the terms defined in the figure, the source is the arterial segment adjacent (and downstream) to the source coordinate, and a leaf is the arterial segment adjacent (and upstream) to a leaf coordinate. Sample diameter values from the model are shown next to arterial segments (see Materials and methods). B) Diagram defining the local and global branching angle. The local angle is the angle between the two children segments very near the branching junction. The global angle is the angle between the branching junction and the endpoints of the children segments.

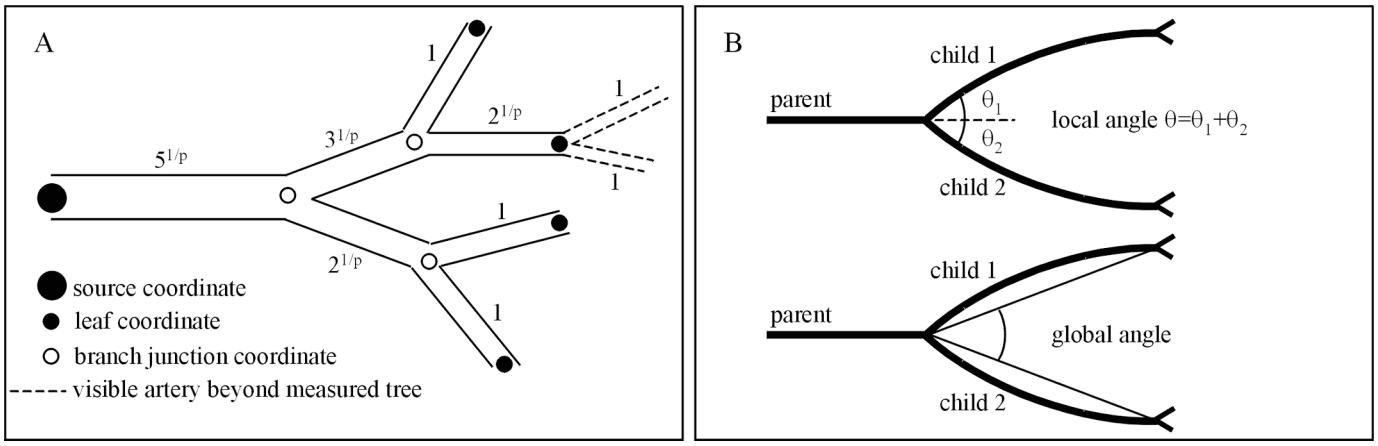

Fig. 2. Segments in trees of different topologies. Although the leaf segments of trees (A) and (B) can be put into correspondence with one another, as can the sources, the segments in between cannot. For example, a corresponds to neither c nor d. It is for this reason that the d^p rule must be used to set the diameter values for non-leaf segments. [See Cherniak et al. (1999) for more discussion on the nature of the alternative topologies.]

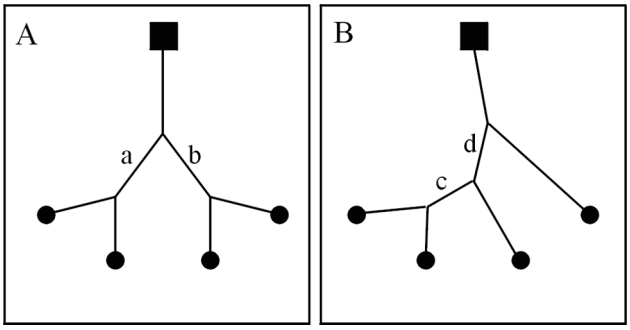

area (S) of the artery (Murray 1927; Kamiya and Togawa 1972). Any pair of these principles are generally not equivalent; however, if one assumes Murray's Law (p = 3), then (P) and (V) are equivalent, as are (D) and (S) (Zamir 1978).

Consider as a simple case a tree with just two leaves (i.e., a single bifurcation), where the tree geometry is characterized completely by the two junction branch angles θ_1, the downstream angle between child 1 and the parent, and θ_2, the downstream angle between child 2 and the parent (see Fig. 1B). Each of the four optimality principles results in an equation for the total branch angle θ ($= \theta_1 + \theta_2$) of the form (Zamir 1976*a*, 1978):

[1] $$\cos\theta = (w_0^2 - w_1^2 - w_2^2) / (2\, w_1\, w_2)$$

where w is the weight computed according to the optimality principle selected, subscript 0 refers to the parent segment, and subscripts 1 and 2 refer to the two child segments. Equation [1] is exactly the triangle of forces law that describes the resulting angle of three strings tied together in a plane under respective tensions, or weights, w_0, w_1, and w_2. The weight under (P) is given by $w_i = f_i^4 / d_i^8$, where f denotes the volumetric flow rate and d the diameter. Similarly, that for (D) is $w_i = f_i^2 / d_i^4$, that for (V) is $w_i = d_i^2$ and that for (S) is $w_i = d_i$. With an assumption of flow proportional to d^p as discussed earlier, one can rid the equations for (P) and (D) of the dependence on flow.

We directly tested only the principles of minimum volume (V) and surface area (S). This is because if one assumes that the flow in a segment is proportional to d^p for an exponent p ϵ [2,3], the predicted tree layouts via optimality principles (P) and (D) are similar to those predicted by (S), and we will discover that (S) is highly disconfirmed by the data in such a way that (P) (when p is not near 3) and (D) (no matter the value of p) are expected to also be disconfirmed. To see this in the simplest case we may consider a single symmetrical junction ($\theta_1 = \theta_2$, $d_1 = d_2$ and $f_1 = f_2 = f_0 / 2$), presume the d^p rule, and ask what are the predicted angles for values of the exponent p ϵ [2,3]. The equations for all four principles become functions of p only, and they are, respectively:

[2] (P) $\theta = \text{acos}(2^{3-8/p}-1)$

[3] (D) $\theta = \text{acos}(2^{1-4/p}-1)$

[4] (V) $\theta = \text{acos}(2^{4/p-1}-1)$

[5] (S) $\theta = \text{acos}(2^{2/p-1}-1)$

Figure 3 shows the graphs of the optimal angle according to each principle as a function of p, and one can see that except when p is near 3, both (P) and (D) predict roughly similar or higher branch angles than (S). We found that (V) is the best predictor of tree geometry, and that it succeeds most in human coronary arteries when p is around 2.6. Only (P) ever performed similarly to (V), and this only occured when (V) is at a suboptimal value for p (namely p = 3). This superiority of (V) and, for exponents p near 3, of (P) was confirmed by Zamir (1986) who reported that for p = 3 (V) and (P) outperformed (S) and (D) over a large range of arterial junc-

Fig. 3. Branch angle versus exponent p. Optimal branch angle (in degrees) for symmetrical junctions via the four different optimality principles (P), (D), (S), and (V) as a function of p from the d^p rule.

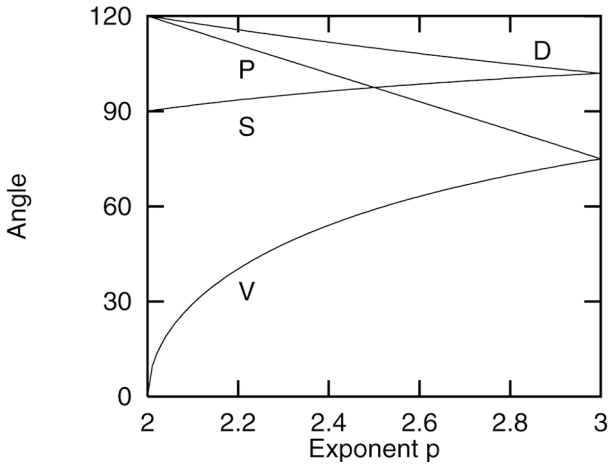

tions, human and non-human. Similar conclusions follow from asymmetrical junctions as well.

The reason why (S), (P), and (D) are poor predictors of tree geometry over the exponent range $p \in [2,3]$ is that they predict branch angles that are too large. (D) and (S) predict angles greater than 90° over the entire range of p; and (P) predicts angles greater than 90° for all $p < 2.667$, and never gets below about 75°. Yet arterial branching angles fall roughly in the range 60° to 80°. For example, Hutchins et al. (1976) measured 57 human coronary artery branch angles, and one can see from their Fig. 5 that only 8 junction angles are above 90° and that the trend is for a mean within the range 60° to 80°. Zamir et al. (1983) measured 302 arterial junctions in rat, and one can see from their Fig. 7 that the trend is the same, and that only 41 junctions have angles measuring above 90°. Zamir et al. (1984) measured 175 rat coronary artery branch angles and found a mean around 70°, and one can see from their Fig. 5 that 38 are greater than 90°. Zamir and Chee (1986) measured 850 branching sites in human coronary arteries and found an average angle of about 70°, and one can see from their Fig. 7 that 212 have angle measures above 90°. Woldenberg and Horsfield (1983) measured 199 human pulmonary artery junctions and the mean branch angle was about 63° (±12°), and one can see from their Fig. 7 in Woldenberg and Horsfield (1986) that 14 are greater than 90°. Cherniak (1992) found a mean of 78.4° for 5 retinal capillaries from human samples (where p is most likely to be near 3, and under a volume optimization model one would expect angles on this high side). Also, the 127 branch junctions of the 48 human coronary arterial trees we studied in this research had a mean angle measure of 63.3° (± 23.9°), and only 19 were greater than 90°. It was sometimes difficult when peering at a single isolated branch angle to tell whether it looked natural, but we observed that multi-junction trees under surface area optimization, with their larger branch angles, just did not look right.

[One might worry about the volume optimization curve in Fig. 3 going to 0° as p approaches 2. This is only physically realizable if the source segment's starting point is infinitely far from the child segment endpoints. In actual implementations, $p = 2$ means that the angle measure will be that between the two lines drawn straight from the source to the children (i.e., the bifurcation occurs at the source), thus, the (V) curve will bottom out at some point, which may make it difficult to differentiate between models each with low (but different) exponents p.]

Materials and methods

Postmortem anterior-view arteriograms of 33 healthy human hearts were obtained from The Johns Hopkins Hospital Department of Pathology (Baltimore, Md.) autopsy files under the direction of Grover M. Hutchins, M.D. Each was photographed with a charged coupled device (CCD) camera, and converted to graphics interchange format (GIF) files readable by National Institutes of Health (NIH) Image software (Fig. 4). 48 arterial trees were selected from the left main descending and right coronary arteries. A few constraints on the selection of arterial trees were enforced. First, trees were not deemed acceptable if branches within them crossed over one another, although we found that this constraint rarely had to be imposed on our arteriograms. Second, because our optimization algorithms only apply to planar arbors, we avoided choosing trees in the peripheral parts of the arteriogram. By doing so, we confined ourselves to trees lying more closely within the plane of the arteriogram (Fig. 4). Third, because acceptable trees with more than five leaves are rare and it is too computationally expensive to compute globally optimal trees for them, only trees with five or fewer leaves were selected.

Measurements of the geometries of the trees, the source, leaf, and branch junction coordinates, local and global branching angles, and segment diameters were obtained from the digitized images of the arteriograms within the NIH Image software. The contrast and brightness of the arteriograms could be manipulated to aid in the identification of arteries and the determination of their geometries. Measurements were made by the first author, a non-expert arteriogram reader; guidance and advice on this was given by Dr. Peter Dockery of the Department of Anatomy, National University of Ireland, Cork. In the recorded actual geometry of a measured tree, segments were represented as straight, i.e., branch wiggle was ignored. The mean of the actual source segment diameters for all 48 trees was 2.65 mm (± 1.0).

Each leaf diameter of a tree was set as follows: the visible arterial tree below the leaf L (i.e., deeper in the tree) on the x-ray was identified (i.e., leaf L was the source of this tree), the leaves of L's tree were set to diameter 1, and L's diameter was computed from these leaves via the d^p rule (e.g., if there are 3 leaves in L's tree, L acquires diameter $(1^p + 1^p + 1^p)^{1/p} = 3^{1/p}$). This idealization partially captures the fact that the leaves of the particular chosen tree are not the true terminal leaves of the arterial network, and that changing the exponent p alters them. Figure 1A shows an example of this; the dotted branches are below (i.e., downstream from) one of the leaves, and are used to compute the leaf's "actual" diameter. Thus, in the model, the leaf diameters are not set to the particular diameters of the actual leaves, but are idealized by computing them based on the number of visible leaves further downstream.

Jen-Hsin Huang and Andrew Kahng (1993) developed an algorithm for us that, when given (*i*) the segment diameters, (*ii*) the source and leaf coordinates, and (*iii*) desired topology of the predicted tree, computes the optimal tree geometry within the desired topology connecting the source to the leaves predicted by a volume (V) or surface area (S) optimizing model. A general description of the algorithm is as follows. With the cosine law from eq. [1], the algorithm finds the minimum-cost coordinate for the branch junction for each pair of leaves, i.e., the coordinate between the source and the center of mass of the two leaves such that the angle is as given in eq. [1]. It then treats these branch junctions as leaves, and

Fig. 4. Sample arteriograms and measured trees. The source (square), branch junctions (small circles), and leaves (large circles) are shown for (A) one measured four-leaf tree from a right coronary artery and (B) one measured three-leaf tree from a left anterior descending coronary artery.

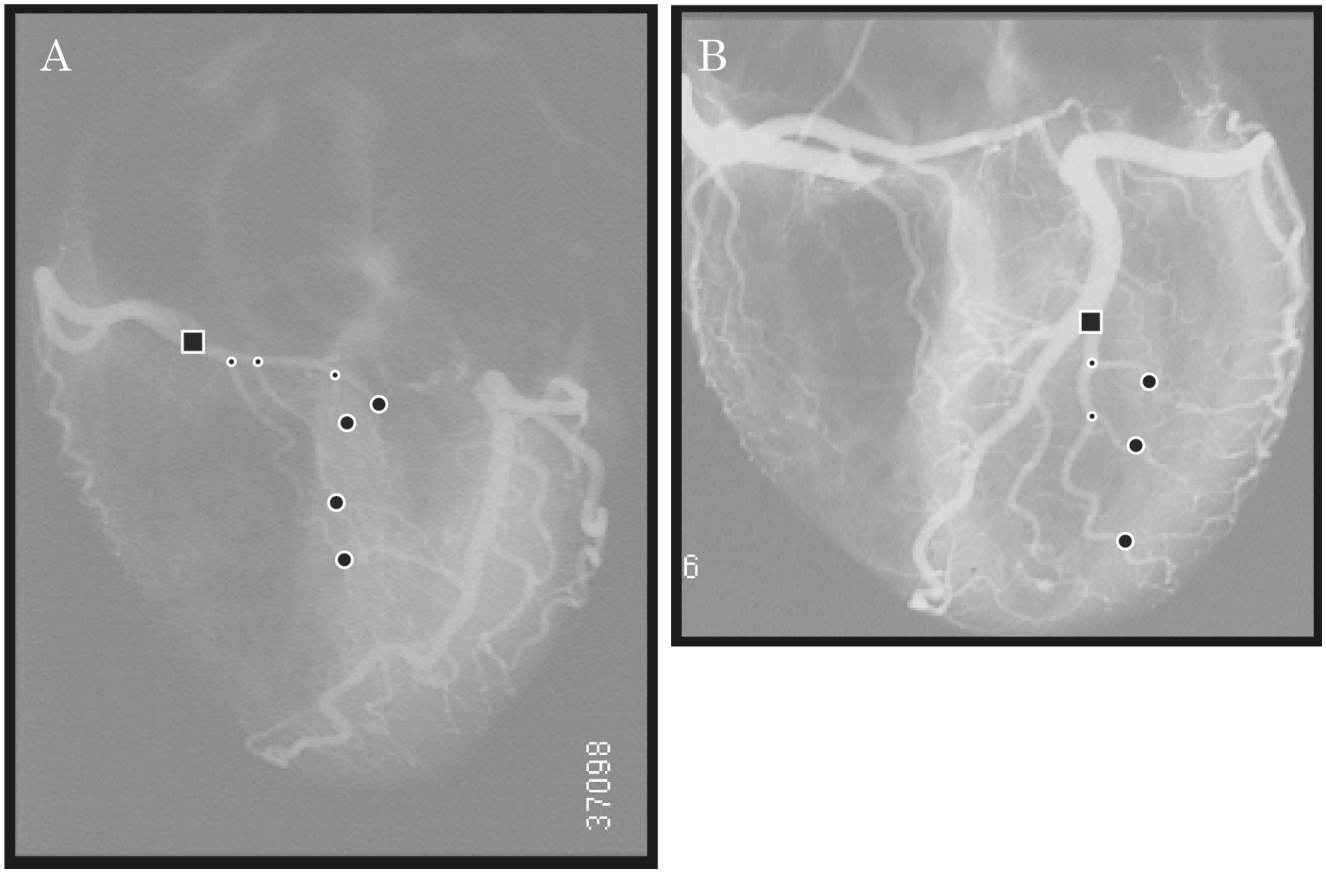

finds the minimum-cost branch junction sites for them. It iterates this, continuing until the source is reached. Du Won Kang created software for us that runs this algorithm over all possible topologies and finds the globally optimum tree geometry. Trees with only 8 leaves have 135 135 distinct topologies, and take over five days to generate on a Pentium 6 400-MHz computer.

For each observed branch junction the local angle (θ, the angle measured at the junction) and the global angle (the angle between the two straight lines connecting the junction to each child's junction, or leaf) were measured (Fig. 1B). Branch bend-in is the phenomenon where the global angle is less than the (local) branch angle, and is ubiquitous in arterial junctions; the mean local branch angle of all 127 junctions measured here was 63.3° (± 23.9°) and the mean global branch angle was 47.4° (± 19.3°), resulting in a mean bend-in of 15.9° (± 22.4°). The best-fit exponent p is the value of p used to obtain segment diameters (via the d^p rule) for which the percent difference between the cost [via (V) or (S)] of the predicted tree geometry and the actual tree geometry is smallest. Because the effective branch angles for the entire actual tree geometry are the smaller global angles rather than the larger local angles, and these smaller branch angles translate to lower values of p [as can be seen in Fig. 3 for (V) and (S)], branch bend-in lowers best-fit values for p. The best-fit values for p for a particular tree were subsequently corrected by (*i*) taking the branch angle from Fig. 3 (for a symmetrical junction) at p, (*ii*) adding to it the mean branch bend-in from the junctions of the tree, and (*iii*) in turn taking the value of p on the x axis of Fig. 3 which corresponded to the sum. The best-fit p below should be assumed to be corrected unless otherwise noted. Negative aspects of this method of correction are that it can be only an approximation, and the mean bend-in is error-prone since it is obtained from the small number of junctions within the one actual tree. On the latter point, it seems nevertheless justified to use only bend-ins from the actual tree since mean bend-in varies widely across arterial trees (from –12.3° to +54.0° in our data).

The sensitivity of the model's predictions to measurement error was tested in the following manner. First, four trees known to be minimum in length (Lewis and Papadimitriou 1978; Bern and Graham 1989) were scanned in, measured in the same manner as were the coronary arteries, and evaluated by the techniques above (except that the minimum length tree was computed instead of the minimum surface area or minimum volume tree). Since the actual trees in this case were optimal, if our measurements were without error the wire length of the measured tree would be identical to our computed optimal tree. The average percent difference between the measured trees and the computed optimal trees was 0.22%. Second, a minimum surface area tree was generated from the source and leaf coordinates of some actual tree. This surface area optimal tree was then used as if it were an actual tree in order to again assess the measurement errors. The surface area error was only 0.000005%. [See Cherniak et al. (1999) for further discussion of the calibration of our methods.]

Table 1 summarizes which quantities are fixed by arteriogram measurement and which were determined by optimization in the model.

Results

The (V) and (S) globally optimum tree geometries were

Table 1. The role of quantities in the model.

Fixed by arteriogram measurement	Determined by the model
Source coordinate	Topology
Leaf coordinate	Branch junction coordinates
Leaf diameters[a]	Non-leaf segment diameters (including source)

[a]See Materials and methods.

computed for each tree over all values of the exponent p ∈ [2,4] at intervals of 0.1 (and also at p = 2.05), and the best-fit p found. The mean best-fit (corrected) p for volume optimization over all 48 trees was 2.60 (± 0.64) (the second decimal place arises from the branch bend-in correction). For surface area optimization it was invariably p = 2, uncorrected, but it was not at a minimum-value trough as in the case for volume, so the best-fit exponent p was actually < 2; consequently we did not correct this p. The reason for the value p = 2 for surface area is that, as Fig. 3 shows, (S) predicts the smallest angles when p = 2 (from the allowable interpretable range [2,3]), and these small angles best agree with the data.

The volume and surface area errors from the actual tree geometry depend on the number of leaves: a greater number of leaves tends to yield greater error, since, intuitively, there is more latitude for the model to fail. Table 2 shows the mean best-fit cost error (percent difference between the cost of predicted and actual geometry) for (V) and (S) for trees of the same number of leaves. In every case volume costing did considerably better than surface area, coming in with errors at a few percent for (V) compared with errors in the teens for (S). On a tree by tree basis, (V) always had a lower error than (S), so this is a highly significant effect ($P < 0.001$).

Figure 5 shows six representative actual tree geometries (in dotted lines) and (in solid lines) the best-fit global optimum volume (B) and surface area (C) geometries for them, as well as the best-fit optimal volume geometry within the actual topology (A). One can see that the optimal tree geometries in the A and B boxes of Fig. 5 are qualitatively similar to the actual tree geometry, while the global surface area-optimizing geometries seem qualitatively dissimilar and unnatural, with branch angles that are too large and branch junctions that occur too near the leaves.

Within a volume-optimizing model we may compare different exponents p. The globally volume-optimum tree geometry was computed for each tree under laminar and turbulent modelsi [i.e., run at p such that the corrected value is 3 and 7/3, respectively (see Discussion)]. The turbulent model predicts tree geometries with lower volume error than the laminar model in 35 of the 48 trees (significance of $P < 0.01$). Table 3 shows the mean errors as a function of the number of leaves, and Fig. 6 depicts the graph showing that the turbulent model is just slightly inferior to the best-fit p, and that the laminar model is more significantly inferior.

Figure 7 shows four actual tree geometries (in dotted lines) and (in solid lines) the best-fit global volume-optimum geometry (B), the turbulent global volume-optimum geometry (A), and the laminar global volume-optimum geometry (C). Compared with surface area in Fig. 5C, all three here did well, and qualitatively do not look too unnatural (with the exception of 1C). To the extent that p = 3 does not do poorly, the single principle of power optimization under a Poiseuille model of fluid flow, allowed to determine both the diameters and tree geometries, is not too poor a predictor of tree geometry, with a gain in parsimony. Future research might concentrate on smaller diameter arterial trees to see whether the best-fit p in such cases is nearer to 3.

Fig. 5. Volume and surface area qualitative comparisons. Each of the six boxes depicts a different human coronary artery tree (scale bar = 1 cm); each is from the left descending artery except for (3), which is from the right main artery. This set was chosen to be roughly representative of the full data set. The dotted trees within a box are identical for A, B, and C and represent the actual tree geometry with branches straightened. The solid tree in B for each box is the globally volume-optimizing tree geometry at the best fit exponent p, where the tree may possess a possibly different topology than that of the actual tree. The value of p is shown, as is the percent error between the volume cost of the optimal tree and the actual tree. The solid tree in A for each box is the volume-optimizing tree geometry within the same topology as the actual tree using the best-fit exponent p from B. If the best topology is the actual one, then A and B are the same. The percent error between the volume cost of this tree and the actual tree is shown. The solid tree in C for each box is the globally surface area-optimizing tree geometry, over all exponents p (which is always minimum at p = 2). The percent error between the surface area cost of this predicted tree and the actual tree is shown. When the number of dots on a leaf L is greater than one, the number of dots denotes the number of leaves below L in the arteriogram.

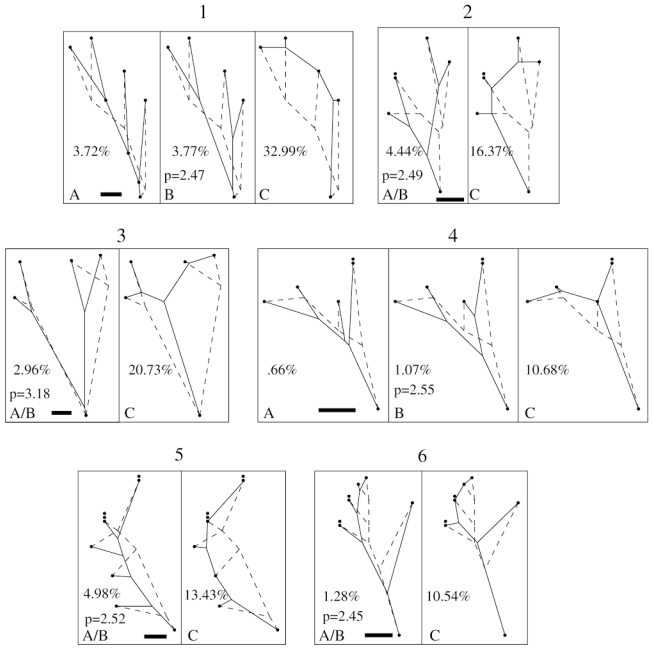

Discussion

Computing the globally volume-optimizing tree geometry is a variation on the classical Steiner tree problem (Bern and Graham 1989) from graph theory which seeks to find the wire length-minimizing tree geometry. The Steiner tree

Table 2. Performance of volume and surface area models.

No. leaves	No. trees	volume error, %	surface area error, %
2	8	0.77 ± 1.12	6.53 ± 2.89
3	8	3.99 ± 4.25	15.13 ± 7.34
4	24	4.19 ± 3.35	19.11 ± 8.89
5	8	5.39 ± 3.27	17.15 ± 7.72

Note: Mean volume and surface area errors of globally optimum tree geometries at best-fit exponents are shown.

Table 3. Performance of turbulent and laminar volume models.

No. leaves	No. trees	turbulent volume error, %	laminar volume error, %
2	8	1.44 ± 1.32	2.13 ± 2.00
3	8	4.40 ± 4.33	5.66 ± 5.23
4	24	4.96 ± 3.69	7.65 ± 4.99
5	8	5.99 ± 3.60	7.89 ± 6.34

Note: Mean volume errors of globally optimum tree geometries for turbulent (p = 7/3) and laminar (p = 3) models are shown, compared with observed artery arbors.

Fig. 6. Error of volume model versus number of leaves. Mean global volume-optimum tree geometry errors for laminar, turbulent, and best-fit p are compared.

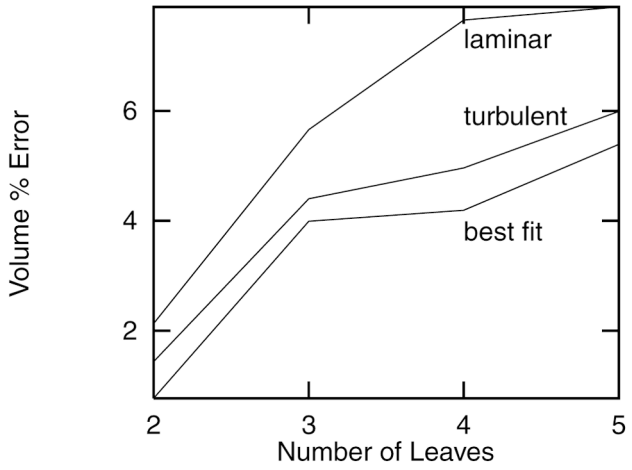

problem is known to be NP-hard (Lewis and Papadimitriou 1978; Garey and Johnson 1979), which strongly suggests that the time needed to solve problems grows exponentially with the size of the problem instance; this, in turn, means that the Steiner tree problem is only tractable for relatively small problem instances. It is therefore implausible to suppose that arterial trees are actually globally optimized, as pleasing and elegant as the idea might be. Arterial geometry is not driven by a computationally sophisticated floorplan, and even if it were, the resources required to compute the optimal geometry for large portions of the arterial network (say, a few hundred-leaf tree) are super-astronomical. This leads to the question via what sort of mechanism might arterial trees be achieving near-perfect global volume-optimal geometries? As noted earlier, eq. [1] is the vector-mechanical equation governing three strings tied together and pulling with weights w_0, w_1 and w_2. As discussed in Cherniak (1992), a mechanism leading to each of the three junction segments pulling on the junction with tension proportional to its cross-sectional area would result in volume-optimizing branch angles as set by eq. [1].

The second major observation is that, for the multi-junction arteries studied here, the best-fit exponent for the d^p rule fluid equation is 2.60, well below the exponent of 3.0 for Murray's Law (and even the turbulent exponent of 2.33 leads to lower errors than the exponent 3.0). Although Murray's Law has been confirmed for a large variety of arteries [see Sherman (1981) for a summary of research confirming Murray's Law prior to 1981, LaBarbera (1990) for data in the 1980s; a few more recent papers include Wang et al. (1992), Rossitti and Löfgren (1993), and Rossitti and Frisén (1994)], it is well known that the assumptions behind Murray's Law stating that blood flow obeys Poiseuille's Law are questionable. In particular Murray's Law assumes that fluid flow is laminar and steady, neither of which can always be expected. For example, flow in larger arteries, being nearer to the heart, is more pulsatile, and the optimal diameter relationship is theoretically area-preserving (West et al. 1997): $d_0^2 = \Sigma d_i^2$. Flow may well be turbulent in larger arteries, in which case the flow rate is theoretically proportional to the diameter raised to the power of 7/3 rather than the laminar exponent of 3 (Uylings 1977), and the diameter relationship becomes $d_0^{7/3} = \Sigma d_i^{7/3}$. And in arteries generally, despite the fact that turbulent flow may not be present, it is possible that the appropriate exponent is below 3 (Roy and Woldenberg 1982; Rossitti 1995).

Furthermore, there exist data confirming lower exponents. Miller (1893) found an exponent of 2.61 for dog lung arteries. Mandelbrot (1977) summarized earlier data in the literature and concluded that the exponent for arteries generally tended to be 2.7. Although Hutchins et al. (1976) found a mean of 3.2 for healthy left main human coronary arteries, they found that for unhealthy left main coronary arteries and other healthy epicardial coronary arteries the mean exponent hovered around 2.7. Suwa et al. (1963) found a mean exponent over a large variety of arterial junctions of around 2.7, and in particular for coronary junctions with diameters greater than and less than 1 mm means of 2.66 and 2.82, respectively. Arts et al. (1979) found that for canine coronary arteries the exponent was 2.55 (which is the expected expo-

Fig. 7. Turbulent, laminar, and best-fit p qualitative comparisons. Each of the four boxes depicts a different human coronary artery tree (scale bar = 1 cm); the first two are from the left descending and the second two are from the right main artery. These arbors are different from the ones in Fig. 5, and are again chosen to be roughly representative of the full data set. The dotted trees within a box are identical for A, B, and C and represent the actual tree geometry with branches straightened. The solid tree in B for each box is the globally volume-optimizing tree geometry at the best-fit exponent p, where the tree may possess a possibly different topology than that of the actual tree. The value of p is shown as is the percent error between the volume cost of the optimal tree and the actual tree. The solid trees in A and C for each box are the globally volume-optimizing tree geometry under, respectively, a turbulent model (p = 7/3≈2.33) and a laminar model (p = 3). The percent error between the volume cost of these trees and the actual tree is shown. When the number of dots on a leaf L is greater than one, the number of dots denotes the number of leaves below L in the arteriogram.

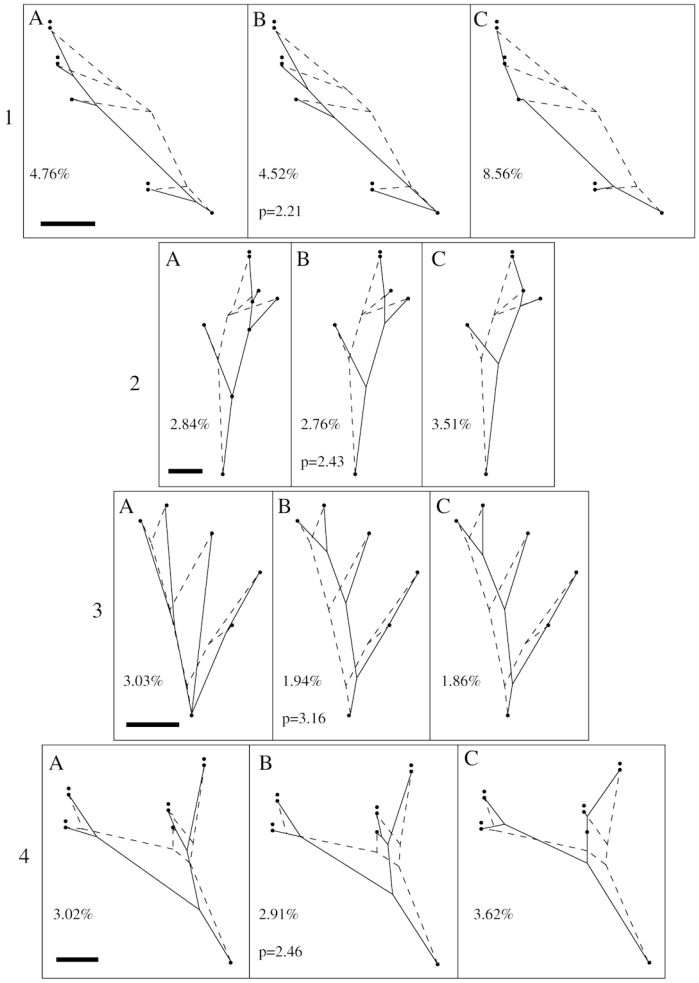

nent if diameters are set to minimize the reflections of pressure waves at bifurcations). Sherman (1981) reexamined the dog small intestinal artery data of Mall (1888) and calculated Σd^p for each depth for exponent values p = 2, 3 and 4. He observed that for p = 3 Mall's values for Σd^p were relatively constant across 15 arterial depths, whereas for p = 2 and 4 there were significant changes in the order of magnitude of Σd^p. However, observing depths 0 through 3 (where the diameters are roughly in the range 0.1– 1.5 mm) we calculated $\Sigma d^{7/3}$ (7/3 being a natural exponent between 2 and 3) from Sherman's Table III, and found that it was more constant in these depths than was Σd^3: Σd^3 was significantly correlated with depth (correlation of –0.98, significance $P < 0.01$) but $\Sigma d^{7/3}$ was not (correlation of –0.20, not significant). We also made similar order of magnitude calculations from the human left lung arterial network data of Huang et al. (1996): from their Tables 5 and 6 we found that the first four depths were more constant for $\Sigma d^{7/3}$ than for Σd^3, although not significantly so (even though the diameters of the segments of these depths are roughly ten times those of the respective depths from Mall; the pulsatile nature of artery segments nearer to the heart as discussed earlier might help to explain this). These latter two observations are roughly consistent with the data of Caro et al. (1971) showing that larger diameter arteries (5–15 mm) have exponents near 2 and the observations of Iberall (1967) that the total cross-sectional area does not change much until arterial diameters are around half a millimeter. In this light, our finding of a best-fit exponent of 2.60 for multi-junction trees with average source diameter 2.65 mm is consistent with the existing trend in the literature for the measured exponent for arterial junctions.

Acknowledgements

We thank Dr. Peter Dockery of the Department of Anatomy, National University of Ireland, Cork, for the use of a

CCD camera and general advice. This work was supported by National Institutes of Mental Health (NIMH) Grant MH49867.

References

Arts, T., Kruger, R.T.I., van Gerven, W., Lambregts, J.A.C., and Reneman, R.S. 1979. Propagation velocity and reflection of pressure waves in the canine coronary artery. Am. J. Physiol. **237**: H469–H474.

Bern, M., and Graham, R. 1989. The shortest-network problem. Sci. Am. **260**: 84–89.

Caro, C.G., Fitz-Gerald, J.M., and Schroter, R.C. 1971. Atheroma and arterial wall shear: observation, correlation and proposal of a shear dependent mass transfer mechanism for atherogenesis. Proc. Roy. Soc. Lond. B **177**: 109–159.

Cherniak, C. 1992. Local optimization of neuron arbors. Biological Cybernetics, **66**: 503–510.

Cherniak, C., Changizi, M.A., and Kang, D. 1999. Large-scale optimization of neuron arbors. Physical Review E **59**: 6001–6009.

Garey, M., and Johnson, D. 1979. Computers and intractability: A guide to the theory of NP-completeness. San Francisco: W. H. Freeman. p. 338.

Hess, W.R. 1917. Uber die periphere regulierung der blutzirkulation. Pflugers Arch. Gesamte Physiol. Menschen Tiere, **168**: 439–490.

Huang, J-H., and Kahng, A. 1993. Variably-weighted steiner minimal trees. Computer Science Department, University of California, Los Angeles.

Huang, W., Yen, B.T., McLaurine, M., and Bledsoe, G. 1996. Morphometry of the human pulmonary vasculature. J. Appl. Physiol. **81**: 2123–2133.

Hutchins, G.M., Miner, M.M., and Boitnott, J.K. 1976. Vessel caliber and branch-angle of human coronary artery branch-points. Circ. Res. **38**: 573–576.

Iberall, A.S. 1967. Anatomy and steady flow characteristics of the arterial system with an introduction to its pulsatile characteristics. Math. Biosci. **1**: 375–395.

Kamiya, A., and Togawa, T. 1972. Optimal branching structure of the vascular tree. Bull. Math. Biophys. **34**: 431–438.

LaBarbera, M. 1990. Principles of design of fluid transport systems in zoology. Science (Washington, D.C.), **249**: 992–1000.

Lewis, H., and Papadimitriou, C. 1978. The efficiency of algorithms. Sci. Am. **238**: 96–109.

Mandelbrot, B.B. 1977. The fractal geometry of nature. New York: W. H. Freeman. p. 460.

Mall, F.P. 1888. Die blut und lymphwege in dunndarm des hundes. Abh. Math.-Phys. Kl. Koniglich Saech. Gessellschaft Wiss. **14**: 151–200.

Miller, W.S. 1893. The structure of the lung. J. Morphol. **8**: 165–188.

Murray, C.D. 1926*a*. The physiological principle of minimum work. I. The vascular system and the cost of blood volume. Proc. Natl. Acad. Sci. U. S. A. **12**: 207–214.

Murray, C.D. 1926*b*. The physiological principle of minimum work applied to the angle of branching of arteries. J. Gen. Physiol. **9**: 835–841.

Murray, C.D. 1927. A relationship between circumference and weight in trees and its bearing on branching angles. J. Gen. Physiol. **10**: 725–729.

Rossitti, S. 1995. Energetic and spatial constraints of arterial networks. Arq. Neuro-Psiquiatr. **53**: 333–341.

Rossitti, S., and Löfgren, J. 1993. Vascular dimensions of the cerebral arteries follow the principle of minimum work. Stroke, **24**: 371–377.

Rossitti, S., and Frisén, J. 1994. Remodelling of the retinal arterioles in descending optic atrophy follows the principle of minimum work. Acta Physiol. Scand. **152**: 333–340.

Roy, A.G., and Woldenberg, M.J. 1982. A generalization of the optimal models of arterial branching. Bull. Math. Bio. **44**: 349–360.

Schreiner, W., and Buxbaum, P.F. 1993. Computer-optimization of vascular trees. IEEE Trans. Biomed. Eng. **40**: 482–491.

Schreiner, W., Neumann, M., Neumann, F., Roedler, S.M., End, A., Buxbaum, P., Müller, M.R., and Spieckermann, P. 1994. The branching angles in computer-generated optimized models of arterial trees. J. Gen Physiol. **103**: 975–989.

Schreiner, W., Neumann, F., Neumann, M., End, A., and Müller, M.R. 1996. Structural quantification and bifurcation symmetry in arterial tree models generated by constrained constructive optimization. J. Theor. Biol. **180**: 161–174.

Sherman, T.F. 1981. On connecting large vessels to small. J. Gen. Physiol. **78**: 431–453.

Suwa, N., Niwa, T., Fukasawa, H., and Sasaki, Y. 1963. Estimation of intravascular blood pressure gradient by mathematical analysis of arterial casts. Tohuku J. Exper. Med. **79**: 168–198.

Uylings, H.B.M. 1977. Optimization of diameters and bifurcation angles in lung and vascular tree structures. Bull. Math. Bio. **39**: 509–519.

Wang, D-B., Blocher, N.C., Spence, M.E., Rovainen, C.M., and Woolsey, T.A. 1992. Development and remodeling of cerebral blood vessels and their flow in postnatal mice observed with in vivo videomicroscopy. J. Cereb. Blood Flow Metab. **12**: 935–946.

West, G.B., Brown, J.H., and Enquist, B.J. 1997. A general model for the origin of allometric scaling laws in biology. Science (Washington, D.C.), **276**: 122–126.

Woldenberg, M.J., and Horsfield, K. 1983. Finding the optimal lengths for three branches at a junction. J. Theor. Biol. **104**: 301–318.

Woldenberg, M.J., and Horsfield, K. 1986. Relation of branching angles to optimality for four cost principles. J. Theor. Biol. **122**: 187–204.

Zamir, M. 1976*a*. Optimality principles in arterial branching. J. Theor. Biol. **62**: 227–251.

Zamir, M. 1976*b*. The role of shear forces in arterial branching. J. Gen. Physiol. **67**: 213–222.

Zamir, M. 1978. Nonsymmetrical bifurcations in arterial branching. J. Gen. Physiol. **72**: 837–845.

Zamir, M. 1986. Cost analysis of arterial branching in the cardiovascular systems of man and animals. J. Theor. Biol. **120**: 111–123.

Zamir, M., and Chee, H. 1986. Branching characteristics of human coronary arteries. Can. J. Physiol. Pharmacol. **64**: 661–668.

Zamir, M., Wrigley, S.M., and Langille, B.L. 1983. Arterial bifurcations in the cardiovascular system of a rat. J. Gen. Physiol. **81**: 325–335.

Zamir, M., Phipps, S., Languille, B.L., and Wonnacott, T.H. 1984. Branching characteristics of coronary arteries in rats. Can. J. Physiol. Pharmacol. **62**: 1453–1459.